Structure of Nanocrystalline TiO_2 Powders and Precursor to Their Highly Efficient Photosensitizer

V. Shklover,*,† M.-K. Nazeeruddin,⊥ S. M. Zakeeruddin,⊥ C. Barbé,⊥ A. Kay,⊥ T. Haibach,† W. Steurer,† R. Hermann,‡ H.-U. Nissen,§ and M. Grätzel⊥

Laboratory of Crystallography and Laboratory for Electron Microscopy I, Swiss Federal Institute of Technology, CH-8092 Zürich, Switzerland; Laboratory of Solid State Physics, Swiss Federal Institute of Technology, CH-8093 Zürich, Switzerland; and Institute of Physical Chemistry II, Swiss Federal Institute of Technology, CH-1015 Lausanne, Switzerland

Received October 24, 1996. Revised Manuscript Received December 5, 1996⊗

Scanning electron microscopy (SEM), high-resolution transmission electron microscopy (HRTEM), and X-ray powder diffraction (XRD) studies on nanocrystalline TiO_2 powders and thin films are presented. The size, shape (mostly exposed faces), and ordering of the TiO_2 anatase particles in the nanocrystalline films are discussed. The use of the topochemical approach, which considers the properties of (nanocrystalline) solids in terms of crystallographic features of (nano)crystals is suggested. The surface area of sensitizer [bis(4,4′-dicarboxy-2,2′-bipyridine)bis(thiocyanato)]ruthenium(II) [abbreviated as (*cis*-Ru(dcbpy)$_2$-(NCS)$_2$] on the semiconductor surface for the different types of anchoring is estimated on the basis of single-crystal X-ray diffraction studies of the esterified form of the complex.

Introduction

The physical properties of nanocrystalline materials may differ from those of bulk materials. The interatomic separations (lattice translations) in nanocrystalline material are nonnegligible as compared with the size of the crystal itself. Special attention has to be paid to the properties of nanocrystalline solids, which are governed by crystal lattice requirements, e.g., the topochemical interaction of nanocrystalline material with organic or metal complex sensitizer. The structure of the interface organic/inorganic was discussed recently by us for the J vs H aggregation in the mixed layered crystals of merocyanine dye.[1] The overlap of π-systems and the nature of the counterion determine the interplanar separations of organic chromophores and the structure of inorganic layer in merocyanine dye salts. These in turn determine the optical properties of merocyanine dye both in the bulk and in thin films. The results obtained were used also in the reverse sense, viz., to deduce the type of dye molecules association with the structure of surface of an inorganic support (or at the of organic/inorganic interface in layered structures). Information can be experimentally determined from the absorption spectra, but such a study is normally quite subtle.

In this work we aimed to study the possible location of metal complex sensitizer on mostly exposed faces to TiO_2 (nano)crystals in photovoltaic cells of new type,[2] based on the crystallographic consideration of the packing of atoms in the crystals of sensitizer and semiconductor. The bipyridine complexes of Ru(II) have been extensively studied because of their possible application in the studies of electron transfer as a function of ligand surrounding in biological systems[3] and as sensitizer coatings.[2,4] The injection of electrons into the conduction band of the (nano)crystalline semiconductor following metal-to-ligand charge-transfer photoexcitation[4] is determined, among other factors, by the surface density of sensitizer molecules on the faces of the (nano)crystals. This dependence may be used for the optimization of the properties of sensitized nanocrystalline materials for the following reasons: (a) the shape and size of the (nano)crystalline support depend on its preparation (see, e.g., the X-ray powder and electron microscopy study[5] of dependence of the particle size and the polymorphic composition of TiO_2 on conditions of hydrothermal synthesis) and (b) the bonding and surface density of sensitizer molecules on the semiconductor surface may be influenced by the modification of the ligand surrounding of metal atoms of sensitizer complexes.

Porous nanocrystalline TiO_2 membranes are often used as a support to form a monomolecular layer of sensitizer. The dependence of the structure and morphology of porous nanocrystalline TiO_2 films on the method of their preparation was discussed earlier.[6,7] The sintering of nanocrystalline TiO_2 particles changes the size, shape, and ordering of the nanoparticles. This in turn may influence the character of bonding and amount

* To whom correspondence should be addressed.
† Laboratory of Crystallography.
‡ Laboratory for Electron Microscopy I.
§ Laboratory of Solid State Physics.
⊥ Institute of Physical Chemistry II.
⊗ Abstract published in *Advance ACS Abstracts,* January 15, 1997.

(1) Nüesch, F.; Grätzel, M.; Nesper, R.; Shklover, V. *Acta Crystallogr.* **1996**, *B52*, 277.
(2) Grätzel, M. *Comments Inorg. Chem.* **1991**, *12*, 93.
(3) Fraser, D. M.; Zakeeruddin, S. M.; Grätzel, M. *J. Electroanal. Chem.* **1993**, *359*, 125.
(4) Péchy, P.; Rotzinger, F.; Nazeeruddin, M. K.; Kohle, O.; Zakeeruddin, S. M.; Humphry-Baker, R.; Grätzel, M. *Chem. Commun.* **1995**, 65.
(5) Cheng, H.; Ma, J.; Zhao, Z.; Qi, L. *Chem. Mater.* **1995**, *7*, 663.
(6) Shklover, V.; Comte, P.; Grätzel, M.; Nesper, R.; Hermann, R. *Proc. Conf. Optical Materials Technology for Energy Efficiency and Solar Energy Conversion XI; Photovoltaics, Photochemistry, and Photoelectrochemistry*; 19−22 May 1992, Toulouse; SPIE Series, Vol. 1729, p 262.
(7) Shklover, V.; Liska, P.; Nazeeruddin, M.; Grätzel, M.; Nesper, R.; Hermann, R. *Proc. Conf. Optical Materials Technology for Energy Efficiency and Solar Energy Conversion XII*, 13−14 July 1993, San Diego, CA; SPIE Series, vol. 2017, p 272.

S0897-4756(95)00502-3 CCC: $14.00

of sensitizer molecules bonded to the nanoparticles. This means that the topochemical conditions of the bonding of sensitizers to nanoparticles may be changed by the sintering process. The consideration of sensitizer−semiconductor interaction within the topochemical approach may help to optimize sensitizer coatings of nanoparticles. The charge collection and transport of electrons across the nanocrystalline membrane to the electrode thus can be improved.[2]

In this work we report on the electron microscopy and X-ray powder diffraction probing of nanocrystalline TiO_2 films and X-ray single-crystal diffraction study of ester of the sensitizer [bis[(4,4′-ethoxycarbonyl-2,2′-bipyridine)(thiocyanato)]ruthenium(II)] ($Ru(etcbpy)_2(NCS)_2$).

Experimental Section

Preparation of TiO_2 Nanopowders. *(1) Synthesis of Colloidal TiO_2.* Titanium isopropoxide (125 mL, 97%, Aldrich) is hydrolyzed at room temperature by its dropwise addition to 750 mL of 0.1 M nitric acid solution under vigorous stirring. A white precipitate is formed instantaneously. Immediately after the hydrolysis, the slurry is heated to 80 °C and stirred vigorously for 8 h in order to achieve the peptisation (i.e., destruction of the agglomerate and redispersion into primary particles). The solution is then filtered on a glass frit to remove nonpeptized agglomerates as well as dust. Water is then added to the filtrate to adjust the final concentration to 5% in weight.

The growth of these particles up to 10−25 nm is achieved under hydrothermal conditions in a titanium autoclave heated for 12 h between 200 and 250 °C. Sedimentation takes place during the autoclaving and the particles are redispersed using a titanium ultrasonic horn (400 W, 15 × 2 s pulses). After two sonications the colloidal suspension is introduced into a rotary evaporator and evaporated (35 °C, 30 mbar) to a final TiO_2 concentration of 11% in weight.

To prevent cracking during film drying and thus render the synthesis of 10 μm thick film possible, poly(ethylene glycol) (molecular weight 20 000, Merck) is added in a proportion of 30−50% of the TiO_2 weight. The resulting paste is stored in a screw thread glass bottle until deposition.

(2) TiO_2 Electrode Preparation. The TiO_2 paste is deposited using a simple doctor blade technique on NipponSheed Glass coated with fluorine-doped SnO_2 layer ($R = 8-10\ \Omega$). The resulting green layer is approximately 100 μm thick. The layer is dried in air for 10 min, followed by a 15 min treatment at about 50 °C. The film is then heated up to 450 °C for 20 min before cooling to room temperature. The thickness of the fired layer is now 8−10 μm.

Synthesis of the Ligand 4,4′-Dicarboxy-2,2′-bipyridine (dcbpy). 4,4′-Dicarboxy-2,2′-bipyridine was synthesized by the slightly modified Sasse method.[8] 4,4′-Dimethyl-2,2′-bipyridine (15.0 g, Me_2bpy) was dissolved in 800 mL of 4 M H_2SO_4 solution at −5 °C to give a 0.081 M solution. $KMnO_4$ solid (32 g, 0.2 M) was added in six portions (one portion every 90 s) with stirring. After half an hour of stirring at the same temperature, another 32 g of (0.2 M) $KMnO_4$ was added in a similar manner. The cooling bath was removed, and the reaction mixture was refluxed for 18 h with stirring. After cooling to room temperature, the solution was filtered using a suction pump. The separated black solid was dissolved in 500−800 mL of 1 M Na_2CO_3 solution. Impurities remaining as insoluble black material were separated by filtering through ordinary filtration funnel. The pH of this filtrate was lowered to 2 by addition of a mixture of CH_3COOH/4 M HCl (1:1 vol/vol). The precipitated white solid was collected on a sintered glass crucible and dried under vacuum at room temperature. The yield was 45−48% (9.0−9.5 g).

The ^1H and ^{13}C NMR spectra show that the product contains less than 2% of 4-COOH-4′-CH_3-2,2′-bpy ligand. This 4-COOH-4′-CH_3-2,2′-bpy impurity was reduced to below 0.1% by refluxing the crude compound (9.3 g in 500 mL) of 6 M HNO_3 solution for 12 h. The solution was poured into a 1-L beaker containing 600 g of ice cubes, the resulting white solid was collected on a sintered glass crucible (G-4) and dried under vacuum at room temperature, yield 8.8 g (95%). Esterification of 4,4′-$(COOH)_2$-2,2′-bpy was carried out by using a conventional procedure.[9]

Synthesis of $Ru(4,4'\text{-}(COOEt)_2\text{-}2,2'\text{-}bpy)_2(Cl)_2$ (1). Solid $RuCl_3(H_2O)_3$ powder (0.13 g, 0.498 mM) was dissolved in 100 mL of ethanol under Ar atmosphere. After stirring for 15 min, 0.293 g (0.976 mM) of 4,4′-$(COOEt)_2$-2,2′-bpy ligand was added. The reaction mixture was refluxed in darkness for 3.5 h with stirring. After this period heating was suspended, and the solution kept under stirring for a further 2 h. The reaction flask was allowed to cool to room temperature and was filtered through sintered glass crucible. The ethanol solvent was evaporated completely under low vacuum. The resulting solid product was washed with 100 ml of 2 M HCl. After the recrystallization from ethanol and diethylether, the yield was 58% (0.2 g).

Synthesis of $Ru(4,4'\text{-}(COOEt)_2\text{-}2,2'\text{-}bpy)_2(NCS)_2$ (2). KNCS (0.4 g, 4.11 mM) was dissolved in 100 mL of ethanol. The solution was transferred into a three-necked flask and purged with Ar for 15 min. Complex **1** (0.13 g, 0.193 mM) was introduced into the flask in darkness. After refluxing for 15 h in darkness with stirring, the reaction mixture was allowed to cool and filtered through a grade-4 sintered glass crucible. The filtrate was evaporated to dryness, the resulting precipitate was washed with water and collected on a sintered glass crucible by suction filtration. The crude complex was recrystallized from dichloromethane and diethyl ether, yield 56% (0.12 g).

Synthesis of $Ru(4,4'\text{-}(COOH)_2\text{-}2,2'\text{-}bpy)_2(NCS)_2$ (3). The complex **2** (0.1 g) was hydrolyzed by refluxing in the presence of 5 mL of triethylamine, water (30 mL), and KNCS (0.4 g) mixture for 8 h. The product was isolated as a neutral salt by acidification (0.05 M, HCl) of the carboxyl groups.

Materials. All solvents used in this study were purest quality obtained from Fluka. Hydrated ruthenium trichloride was purchased from Johnson Matthey and used as received.

Spectral Measurements. UV−visible and fluorescence spectra were recorded on Cary and Spec spectrophotometers, respectively. Infrared spectra were measured as KBr pellets on a Perkin-Elmer 6811 instrument. ^1H and ^{13}C NMR spectra were measured on a Bruker 250 spectrometer. Natural abundance ^{13}C NMR spectra were recorded using D_2O as an external lock.

High-Resolution Transmission Electron Microscopy (HR-TEM). The HRTEM study of the colloidal TiO_2 film heated at 240 °C was performed at 300 kV on Philips CM 30 ST transmission electron microscope equipped with a detector for energy-dispersive X-ray spectrometry (EDX) and a STEM attachment. A thin single-crystal gold film was used as the internal standard for the determination of interplanar distances.

Scanning Electron Microscopy (SEM). The samples were also examined at 30 kV accelerating voltage in a Hitachi S-900 "in-lens" field-emission scanning electron microscope with a standard Everhard-Thornley SE detector and a YAG type BSE detector.

Single-Crystal X-ray Diffraction Study of Complex 2. The data collection for the single crystal **2** of the ester derivative of the sensitizer $[Ru(dcbpy)_2(NCS)_2]$ was performed at 210 K (crystals **2** are unstable under X-ray irradiation) on an Enraf-Nonius CAD-4 diffractometer using Mo Kα radiation (λ = 0.710 73 Å) equipped with a graphite monochromator. Using $\omega/2\theta$ scan technique all reflections in the range $2.92 < \Theta < 30.44°$ were collected using the CAD4-EXPRESS software.[10] The index ranges were $-35 < h < 35$, $-14 < k < 0$,

(8) Launikonis, A.; Lay, P. A.; Mau, A. W.-H.; Sargeson, A. M.; Sasse, W. H. F. *Aust. J. Chem.* **1986**, *39*, 1053.

(9) Maerker, G.; Case, F. H. *J. Am. Chem. Soc.* **1958**, *80*, 2745.

(10) CAD4-EXPRESS. User Manual; Delft Instruments X-ray Diffraction, Delft, 1992.

Table 1. Experimental Details of X-ray Structure Determination of the crystal 2 ($Ru(etcbpy)_2(NCS)_2 \cdot 2CH_3CN$)

formula weight	891.71
crystal color, habit	brown, thin plate
crystal dimensions [mm]	0.3 × 0.2 × 0.05
crystal system	monoclinic
space group	*C*2/*c*
lattice parameters	
a [Å]	25.182(6)
b [Å]	10.229(2)
c [Å]	16.069(2)
β [deg]	102.89(1)
V [Å^3]	4034.85
Z	4
density calc [g cm^{-3}]	1.476
absorption coefficient	
μ (Mo Kα) [mm^{-1}]	0.55
F(000)	1848
T [K]	210
reflections measured	4703
independent reflections, R_{int}	1399, 0.11
observed reflections, $F > 3\sigma(F)$	1046
no. of refined parameters	123
residuals *R*, R_w	0.0785, 0.0968
reflections/parameters ratio	8.5
goodness of fit	1.274

$-22 < l < 0$. Three standard reflections were measured every 1 h for the intensity control and two standard reflections were checked every 100 reflections for the orientation control. The intensities were measured with prescan determined scan speed to reach the ratio $\sigma(I)/I = 0.03$, the maximum measurement time was 50 s/reflection.

The molecule of the complex $Ru(etcbpy)_2(NCS)_2$ occupies a special crystallographic position on the 2-fold axis. The solvent molecule acetonitrile used for crystallization was found in the general position in the difference Fourier synthesis. Consequently the composition of the single crystal **2** is $Ru(etcbpy)_2(NCS)_2 \cdot 2CH_3CN$. Experimental details and results of the structure refinement are summarized in Table 1. The atomic coordinates of non-hydrogen atoms are given in the Table 2. Programs of SHELXTL PLUS[11] were used for data reduction, structure solution, and refinement.

X-ray Powder Diffraction Study. The powder diffraction patterns of TiO_2 films on the glass support were recorded on a Scintag powder X-ray diffractometer with a Ge detector using Cu-radiation.

Results and Discussion

UV−Visible Spectra. The absorption spectral data of complexes **1**, **2**, and **3** in the UV visible region are presented in Table 3. All the complexes show intense visible bands in the 540 nm region. In the UV, the complexes show an intense band at 314 nm with a shoulder at 298 nm. This band is due to ligand $\pi-\pi^*$ transitions.[12] The lowest energy bands originate from metal-to-ligand charge transfer (MLCT), corresponding to transitions from the metal t_{2g} to the ligand π^* orbital.[13,14] The longer wavelength band of complex **2** is 30 nm red-shifted when compared to unsubstituted bpy complexes of the similar type. This red-shift is mainly induced by the electron-withdrawing nature of the $COOC_2H_5$ groups at the 4,4′-position, which lowers the energy of the π^*-orbital of the ligand. The lowest energy MLCT band in complex **2** blue-shifts by 6 nm upon hydrolysis of the ester group. Deprotonation of the COOH groups in complex **3** causes a blue-shift of the higher energy $\pi-\pi^*$ CT band (314−308 nm) and low-energy MLCT band (536−500 nm). The blue-shift is due to an increase in the energy of the LUMO of the ligand, causing the $\pi-\pi^*$ and $d\pi-\pi^*$ transitions to occur at higher energies. A quantitative analysis of the absorption and emission spectral changes as a function of pH yielded respectively the ground- and excited-state pK_a values of the carboxy groups.[14]

Data on the dependence of the absorption spectrum with the solvent polarity are presented in Table 3. Charge-transfer states in general are solvent sensitive. The lowest MLCT band in complex **3** shows a blue-shift of 40 nm going from aprotic solvent such as DMSO to protic solvent such as H_2O. There are two factors that can be responsible for the observed blue-shift: (i) H-bonding to the lone-pair electrons of the nitrogen/sulfur, previously noted for cyanocomplexes of Ru and other related systems; (ii) an effect due to the deprotonation of the carboxy groups. Since the observed shift in **2** is only 6 nm, the second effect, viz., deprotonation of carboxy groups are likely to be responsible for the blue-shift of the low-energy MLCT band.

Luminescence. The complexes **2** and **3** are luminescent in fluid solution at room temperature. Complex **2** shows an emission maximum at 875 nm in acetonitrile

Table 2. Atomic Coordinates (×10^4 for Ru, S, O, and N, ×10^3 for C and Atoms of Solvent) and Equivalent Displacement Parameters U_{eq} (Å^2 × 10^3) of Non-Hydrogen Atoms in the Crystal 2

atom	*x*	*y*	*z*	U_{eq}[a]
Ru	0	4714(4)	1/4	11(1)
S	863(3)	1132(9)	1363(4)	42(4)
O(1)	1649(7)	5724(25)	6542(11)	56(6)
O(2)	2188(6)	4451(21)	5970(9)	36(4)
O(3)	−1441(7)	8753(22)	4700(10)	40(5)
O(4)	−622(7)	8654(2)	5608(10)	41(5)
N(1)	−316(7)	6055(23)	3197(10)	14(5)
N(2)	597(6)	4847(25)	3562(9)	19(4)
N(3)	370(7)	3237(24)	1953(11)	16(5)
C(1)	56(1)	236(3)	170(1)	19(6)
C(2)	−3(1)	624(3)	399(1)	15(5)
C(3)	49(8)	563(3)	419(1)	14(5)
C(4)	108(1)	418(3)	371(1)	24(6)
C(5)	146(1)	423(3)	447(1)	25(6)
C(6)	137(1)	505(3)	510(1)	25(6)
C(7)	89(1)	574(3)	498(1)	25(6)
C(8)	−21(1)	710(3)	454(1)	22(6)
C(9)	−73(1)	762(3)	428(1)	16(6)
C(10)	−102(1)	744(3)	348(1)	30(7)
C(11)	−79(1)	663(3)	296(1)	18(6)
C(12)	176(1)	514(3)	597(1)	31(6)
C(13)	−96(1)	847(3)	491(1)	34(7)
C(14)	258(1)	437(4)	678(2)	70(10)
C(15)	280(1)	304(4)	684(2)	67(10)
C(16)	−82(1)	941(4)	623(1)	48(8)
C(17)	−59(1)	1067(6)	638(2)	121(16)
N(4)[b]	191(1)	263(4)	857(2)	78(9)
C(18)[b]	230(1)	322(4)	889(2)	57(9)
C(10)[b]	277(1)	392(4)	927(2)	55(9)

[a] Equivalent isotropic coefficients *U* defined as one-third of the trace of the orthogonalized U_{ij} tensor. [b] Atom of the solvate acetonitrile molecule.

(11) Sheldrick, G. M. *SHELXTL PLUS. VAX/VMS Version*; Siemens Analytical X-ray Instruments Inc., Madison, WI, 1990.

(12) Stone, M. L.; Crosby, G. A. *Chem. Phys. Lett.* **1981**, *79*, 169. Bryant, G. M.; Fergusson, J. E.; Powell, H. K. J. *Aust. J. Chem.* **1971**, *24*, 257. Sauvage, J.-P.; Collin, J.-P.; Chambron, J.-C.; Guillerez, S.; Coudret, C.; Balzani, V.; Bargelletti, F.; De Cola, L.; Flamigni, L. *Chem. Rev.* **1994**, *94*, 993.

(13) Nazeeruddin, M. K.; Humphry-Baker, R.; Pechy, P.; Rotzinger, F. R.; Grätzel, M. *Abstr. Tenth International Conference on Photochemical Conversion and Storage of Solar Energy*; Interlaken, July 24−29, 1994, p 201.

(14) Shimidzu, T.; Iyoda, T.; Izaki, K. *J. Phys. Chem.* **1985**, *89*, 642. Giordano, P. J.; Bock, C. R.; Wrighton, M. S. *J. Am. Chem. Soc.* **1978**, *100*, 6960. Nazeeruddin, M. K.; Kalyanasundaram, K. *Inorg. Chem.* **1989**, *28*, 4251.

Table 3. Electronic Spectral Data of the Complexes 1, 2, and 3 in Solution at Room Temperature[a]

complex	solvent	MLCT	MLCT	p−p* CT
$[Ru(4,4'\text{-}COOEt\text{-}2,2'\text{-}bpy)_2(Cl)_2]$ (**1**)	H_2O	540 (9.8)	402 (8.8)	318 (30.0)
	C_2H_5OH	568 (11)	420 (11.4)	318 (32.3)
	DMSO	586 (8.7)	434 (8.7)	324 (26.6)
$[Ru(4,4'\text{-}COOEt\text{-}2,2'\text{-}bpy)_2(NCS)_2]$ (**2**)	H_2O[b]	544 (8.8)	408 (10.2)	316 (29.0)
	C_2H_5OH	544 (9.4)	406 (9.9)	316 (32.9)
	DMSO	550 (9.0)	414 (9.5)	320 (27.8)
$[Ru(4,4'\text{-}COOH\text{-}2,2'\ bpy)_2(NCS)_2]$ (**3**)	H_2O	500 (13.1)	372 (12.4)	308 (49.0)
	C_2H_5OH	538 (13.1)	398 (13.0)	314 (49.4)
	DMSO	542 (13.2)	400 (13.0)	318 (45.7)

[a] Wavelengths are in nm, the values in parentheses are $\epsilon \times 10^3$ [M^{-1} cm^{-1}]. [b] In 0.1% DMSO + H_2O.

Table 4. ^{1}H NMR Chemical Shifts for Free Ligands and Complexes and Coordination-Induced Shifts (CIS = $d_{complex} - d_{free}$) for H-6 Protons[a]

ligand or complex[b]	6	6′	5	5′	3	3′	CH_2,CH'_2	CH_3,CH'_3	cis
etcbpy	9.41		8.45		9.49		4.97	1.95	
dcbpy	8.78		7.87		8.40				
1	10.14	8.09	7.55	7.46	8.79	8.65	4.47; 4.33	1.43; 1.2	0.73
2	9.62	8.21	7.54	7.53	8.85	8.69	4.48; 4.33	1.43; 1.29	0.21
3	9.55	7.82	8.22	7.52	8.94	8.77			0.77

[a] In ppm with respect to TMS. Positive cis values refer to downfield shifts. [b] Complexes **1**, **2** and ligand eetcbpy were recorded in CD_2Cl_2, complex **3** and ligand etcbpy were recorded in D_2O containing 0.01 M NaOH. The primed notation indicates the protons of the pyridine ring trans to an NCS ligand.

solution with an emission lifetime of 125 ns. The complex **3** has an emission maximum at 755 nm with a shorter lifetime of 50 ns. It is noteworthy that complex **3** with the higher energy emission maximum has a shorter lifetime than **2** (with the low-energy emission maximum). The emission quantum yield of **2** (ϕ_{em} = 0.0005) is approximately 2.5 times higher than that of complex **3** (ϕ_{em} = 0.0002). The red-shift of the low-energy absorption, emission maxima of **2** compared to complex **3** is due to the low-energy π^* orbital of ester form of the ligand compared to 4,4′-COOH-2,2′-bpy ligand.

These assignments are further corroborated by electrochemical studies. Cyclic voltammograms of **2** and **3** were measured in DMSO containing 0.1 M tetrabutylammonium trifluoromethanesulfonate as supporting electrolyte. In the potential range +1.2 to −1.5 V the complex **2** shows one quasi-reversible oxidation wave at +0.9 V and two reversible reduction waves at −0.98 and −1.1 V vs Ag/AgCl. These are assigned to the oxidation of Ru(II) to Ru(III) and bpy/bpy-based reductions, respectively. The bpy-based reduction potentials in **3** are at −1.1 and −1.22 V vs Ag/AgCl which are 120 mV more negative shifted than that of **2**.

^{1}H NMR Spectroscopy. The ^{1}H NMR spectrum data of **1**, **2**, and **3** were given in Table 4. Proton NMR spectra of complexes **1**, **2**, and **3** show six resonances in the aromatic region, corresponding to two different bpy ring protons, in which two pyridine rings are trans to NCS ligands and the remaining two are trans to each other. In complex **2**, the coordination geometry about each Ru is imperfectly octahedral (see discussion below), with bipyridyl bite angle of 78.8°.

Herein we attempt to correlate the coordination-induced chemical shift vs bond length. The Ru−N bond lengths show significant variations. In an axial position, two pyridine rings are trans to each other, showing Ru−N bond length 2.011 Å, whereas the pyridine rings trans to NCS show 2.041 Å. This indicates that the NCS ligand is a good π-acceptor. In transition-metal complexes, bond lengths depend on two effects. First, the extent of the donation from ligand to metal, which is an indirect measure of the delocalization of electron density from ligand to metal via the nitrogen lone pair. The second effect results from the metal back bonding of t_{2g} electron density to the empty π^* orbital of the ligand. In ^{1}H NMR, the chemical shifts are related to the extent of electron density around the proton. On the basis of the above discussion, it is tempting to invoke the assignment of down-field-shifted proton resonances corresponding to pyridine rings trans to each other, and the remaining three proton resonances to pyridine rings trans to NCS ligand. This assignment is also consistent with the literature.[15]

Coordination via N or S(Se). The reaction of chalcogenocyanate ions with transition-metal complexes having weakly coordinated ligands yields chalcogenocyanate complexes. The coordination mode of chalcogenocyanate also depends on the presence of other ligands around the metal center and the nature of the metal. The possibility of formation of S or Se bonded compounds was discussed for M(II) complexes with π-acid ligands such as CN^-, bpy, or PPh_3.[16] The presence of strong σ-donor ligands such as NH_3 around the metal favors the S/Se coordination. The problem of determining the bonding modes of coordinated ambidentate ligands has been addressed by IR and Raman technique. The NCS group has two characteristic modes ν(NC) and ν(CS) that have been frequently considered as diagnostic. In polypyridyl complexes, the ν(CS) stretching mode cannot be assigned with certainty because of pyridine ring stretches showing in the same region.

We herein report proton decoupled ^{13}C NMR spectra **2** and **3**, which are particularly useful for determining the N- or S-bonded coordination of the NCS ligand. It has been reported that S coordination of NCS ligand-to-transition metals shields the carbon atom much more than N coordination.[17] The S-coordinated NCS ligands

(15) Constable, E. C.; Seddon, K. R. *Chem. Commun.* **1982**, 34.
(16) Wajda, S.; Rachlewicz, K. *Inorg. Chim. Acta* **1978**, *31*, 35. Gutterman, D. F.; Gray, H. B. *Inorg. Chem.* **1972**, *11*, 1727. Hubener, R.; Abram, U. *Inorg. Chim. Acta* **1993**, *211*, 121.
(17) Kargol, J. A.; Cresely, R. W.; Burmister, J. L. *Inorg. Chem.* **1979**, *18*, 2532.

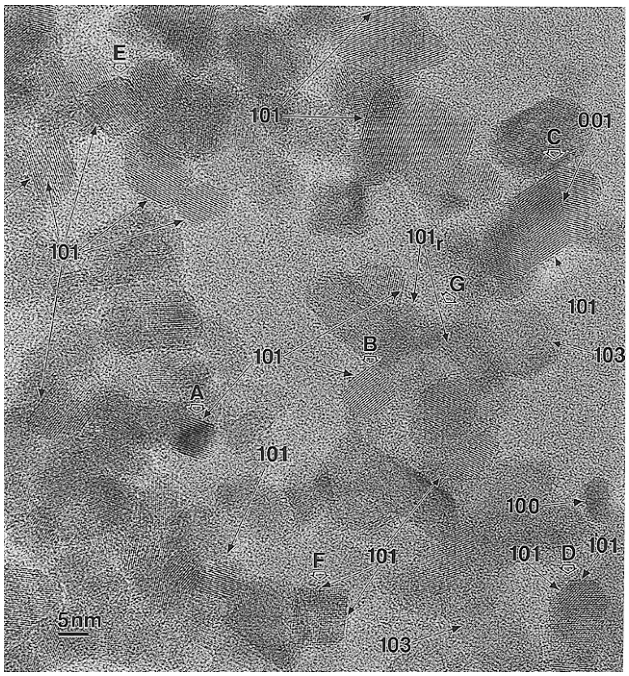

Figure 1. HRTEM micrograph at 300 kV of the colloidal TiO_2 film heated at 240 °C. The designations A−G are explained in the text.

show carbon resonances at 112−128 ppm, whereas the ^{13}C chemical shifts of N-bonded NCS groups are in the range 130−140 ppm. The ^{13}C NMR spectra of complexes **2** and **3** show six pairs of resonances corresponding to two different bpy ligands and one single peak at 134 ppm. On the basis of the literature data, one can unambiguously assign the 134 ppm resonance peak due to the carbon of N-coordinated NCS. Consequently, the two NCS ligands are nitrogen bonded as has been found for all structurally characterized Ru−NCS complexes.[18]

Size, Shape, and Ordering of Particles in TiO_2 Films. The HRTEM micrograph of the colloidal TiO_2 film autoclaved at 240 °C shows quite broad particle size distribution from 5 to 40 nm (Figure 1). Even very small particles of ~5 nm size exhibit crystalline structure (which could be observed by HRTEM under proper orientation of the crystal grains) and may be well-shaped, see for example, regions A and B on the Figure 1. The crystallinity of very small particles in the film was expected, when one considers the fact that the film was produced from TiO_2 P25 (Degussa) with well-known nanocrystalline structure.[19,20] The size, shape, and crystallinity of the fine TiO_2 nanoparticles depend on the method of preparation of the powder.[5−7] Spherical TiO_2 agglomerates with approximately 6 nm primary structure were produced by the controlled hydrolysis of $Ti(EtO)_4$.[21] The X-ray study of this amorphous powder has shown (local) octahedrally coordinated crystalline order of brookite, composed of fine particles of ca. 6 nm size with an approximate correlation length of 1 nm. The HRTEM study at 400 kV indicates only a contrast, characteristic of amorphous films. The SEM analysis of amorphous TiO_2 powders with particle size of 0.07−0.6 μm, produced by the mentioned controlled hydrolysis of titanium alkoxides, has shown uniform packing of spherical particles ordered into face-centered cubic array with average number of particle−particle contacts greater than 11 per particle. Uniform nanosize rutile and anatase particles were prepared by a hydrothermal method using $TiCl_4$ as starting material.[5]

The fringes of TiO_2 nanocrystallites on Figure 1 allows the identification of crystallographic spacings and their orientation. The fringes corresponding to (101) crystallographic planes of anatase are most frequently observed, and they constitute both large (up to 40 nm) and very fine properly oriented crystallites (5−10 nm). The frequency, good orthogonal orientation of the noncrossing (101) crystal planes to the surface of the pattern may indicate the exposure of crystal faces (010) which are oriented perpendicular to the planes (101).

The measured value of the dihedral angle $\phi \sim 112°$ formed by two crossing fringes (101) ($d = 3.53$ Å, $d(101)^* = 3.52$ Å) and (001) ($d = 2.38$ Å, $d(004)^* = 2.38$ Å) of twinned crystals on the C region of the Figure 1 is close to the calculated value of $\phi = 111.7°$ of the angle between the planes (001) and (101). The face (001) intersect with four (101) planes in the anatase crystal of dipyramidal form (see, e.g., ref 23). The orthogonal orientation of the boundary twin plane (001) and of the fringes of (101) planes to the plane of the grid means, that the plane (100) is parallel to the plane of the pattern.

The traces of the planes (101) of the crystallite D form the angle $\phi \sim 135°$ which nearly coincides with the angle, formed by the faces (101) of the anatase on the face (100). So, the fringe pattern D is oriented perpendicular to the face (010), which is consequently exposed. The (010) face as exposed one was observed also in the HRTEM study of TiO_2 P25 film (Degussa) obtained by the flame hydrolysis of $TiCl_4$.[24]

The fringe spacings found in the G region of the micrograph on the Figure 1 indicate the presence of rutile microcrystals in the studied TiO_2 film ($d = 2.48$ Å, $d(101)_{rutile} = 2.49$ Å [the interplanar separations are from ref 25]). The rutile microcrystals in the region G have small size of ca. 10 nm. The presence of comparable amounts of both anatase and rutile microcrystals in the colloidal TiO_2 films autoclaved at 240 °C is well-known, see, e.g., the SEM and powder diffraction studies.[6,7] The termination of the rutile crystallites with the (001) and (110) planes is quite likely in the samples sintered at 800 °C.[24]

The termination of the anatase nanocrystallites in the TiO_2 colloid film treated at 240 °C with the planes (101), (010), and (to less extent) (001) is quite likely. The resulting habitus of the anatase microcrystals in the film was found by SEM studies presented on the Figure 2. These results do not contradict to the HRTEM study

(18) Herber, R. H.; Nan, G.; Potenza, J. A.; Schugar, H. J.; Bino, A. *Inorg. Chem.* **1989**, *28*, 938.
(19) Spoto, G.; Morterra, C.; Marchese, L.; Orio, L.; Zecchina, A. *Vacuum* **1990**, *41*, 37.
(20) Cerrato, G.; Marchese, L.; Morterra, C. *Appl. Surf. Sci.* **1993**, *70/71*, 200.
(21) Wang, Q. J.; Moss, S. C.; Shalz, M. L.; Glaeser, A. M.; Zandbergen, H. V.; Zschack, P. In *Physics and Chemistry of Finite Systems: From Clusters to Crystals*; Jena, P., et al., Eds.; Kluwer Academic Publishers: Dordrecht, 1992; Vol. II, p 1287.
(22) Barringer, E. A.; Bowen, H. K. *J. Am. Ceram. Soc.* **1982**, *65*, C-199.
(23) In *Klockmanns Lehrbuch der Mineralogie*; Ramdohr, R., Strunz, H., Eds.; Enke Verlag: Stuttgart, 1978.
(24) Martens, J. H. A.; Prins, R.; Zandbergen, H.; Koningsberger, D. C. *J. Phys. Chem.* **1988**, *92*, 1903.
(25) VAX-PDF, Card Retrieval Display System, Version 1.12, JCPDF−International Centre for Diffraction Data, Newton Square, PA 19073−327.

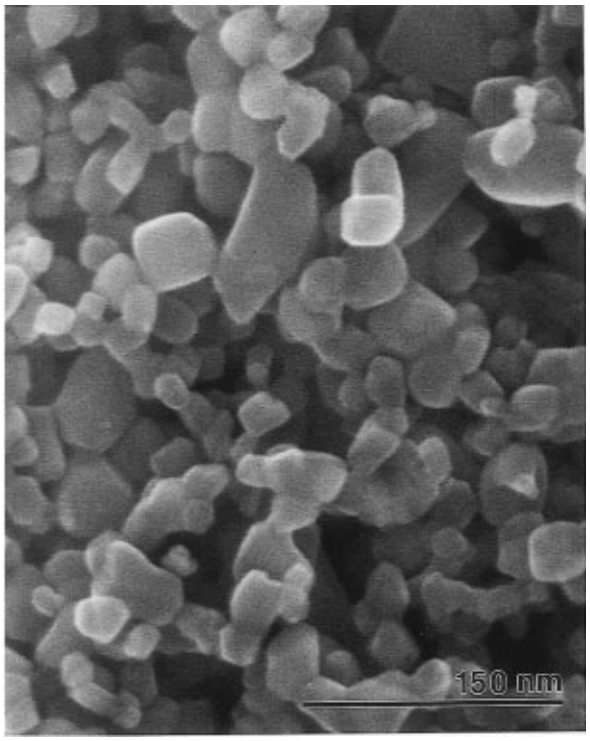

Figure 2. SEM micrograph of the colloidal TiO_2 film heated at 240 °C.

of TiO_2 P25 Degussa: the TiO_2 microcrystals are well-shaped prisms essentially exposing the (101), (010), and (001) faces, the former one being definitively more abundant.[19] The HRTEM study of Rh/TiO_2 catalyst after reduction at 773 K and subsequent passivation have shown that crystallographic planes exposed mostly are (101) crystal faces (the TiO_2 powder with large surface area of 130 $m^2\ g^{-1}$ was prepared by hydrolysis of $Ti(OC_3H_7)_4$ with final calcination at 923 K). Other planes exposed are (001) and (103).[24]

The morphological parameters of particles influence the packing in nanopowder (the packing in colloidal nanocrystalline films depends not only on the nanoparticles shape but more on the presence of surfactant or counterions) and the complicated mechanism of reactions in powders (see discussion[26] of kinetics of powder reactions). Two extreme examples of the influence of the shape of the particles are the packing of pseudospherical ZnO particles with the maximum number of neighbors 12 (Figure 3) and the dense packing of pseudo-square-bipyramidal TiO_2 particles with the maximum number of neighbors four in the equatorial plane (Figure 4). The faces (001) of nanocrystals in the corresponding dense sintered anatase film, consisting of pseudo-square-bipyramidal particles, will be eliminated from the interaction with the sensitizer molecules. (The synthesis of this TiO_2 powder will be described later.)

Three levels of structural organization of "large" TiO_2 nanoparticles can be observed in the Figure 5a–c. The individual pseudospherical particles of ~200 nm size (Figure 5a) are very loosely packed into associates (Figure 5b) which may form very unusual hollow aggregates (Figure 5c).

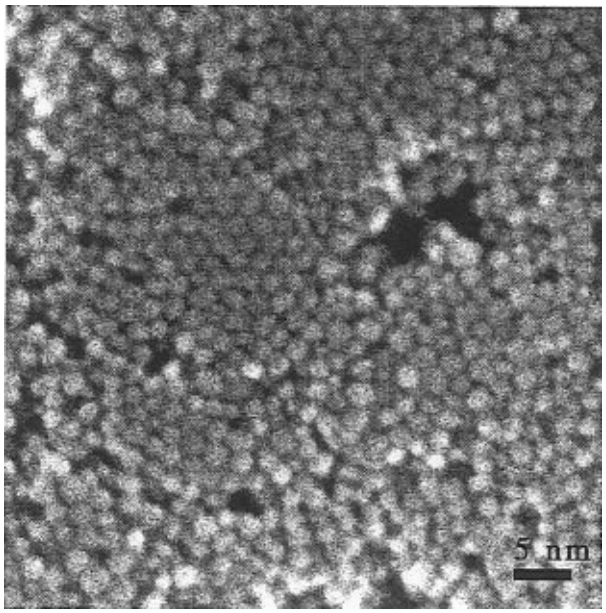

Figure 3. SEM micrograph of ZnO film showing the pseudohexagonal packing of nanoparticles with the maximum number of neighbours 12 (6 in "equatorial" plane).[27]

The precise morphology of the surface of the ZnS pattern in the submicron region is an example of the importance of monodispersity for the formation of highly ordered packing. The film was obtained by the deposition of monodisperse polystyrene microspheres on a glass substrate (using Langmuir–Blodgett film technique), resulting in formation of densely packed monolayers, with subsequent ZnS deposition and removal of polymer. The lattice spacing in the resulting pattern was ~900 nm for the 2 μm diameter polymer spheres.[28]

These examples show a large variability of the structure and morphology of nanopowders. In general, the more favorable the mass-transport processes during sintering, the better is the ordering of nanoparticles or the denser is their packing in the sintering product. On the other hand, the sintering as a minimization of the total surface free energy[29] may influence the electrophysical properties of nanopowders, obtained by nanoconfinement. To retain essential porosity of studied TiO_2 films, only limited sintering at the temperatures not higher as 500 °C was used: ~0.1% depletion with the surface area loss <1%.

The "packing" of quantum confined moieties into nanocomposite bulk materials may be used to define the confinement surface states and the effective charge-carrier density of the bulk.[30] Theoretically, the most perfect packing may be obtained using three-dimensional crystal superlattices as hosts for quantum-confined atom arrays obtained by lattice-controlled intercalation (e.g., in zeolites[30]). The highly ordered TiO_2 films form an example of alternative approach for controlled generating nanocomposite materials consisting of densely packed monodisperse nanoparticles. The implanting Cu ions into fused silica is an example of

(26) Schmalzried, H. *Chemical Kinetics of Solids* VCH: Weinheim, 1995; p 157.
(27) Björksten, U.; Moser, J.; Shklover, V.; Grätzel, M. *Langmuir*, in press.
(28) Lenzmann, F.; Li, K.; Kitai, A. H.; Stöver, H. D. H. *Chem. Mater.* **1994**, *6*, 156.
(29) Schmalzried, H. *Solid State Reactions*. In *Monographs in Modern Chemistry*; Ebel, H. F., Ed.; Verlag Chemie: Weinheim, 1981; p 16.
(30) Stucky, G. D.; Mac Dougall, J. E. *Science* **1990**, *247*, 669.

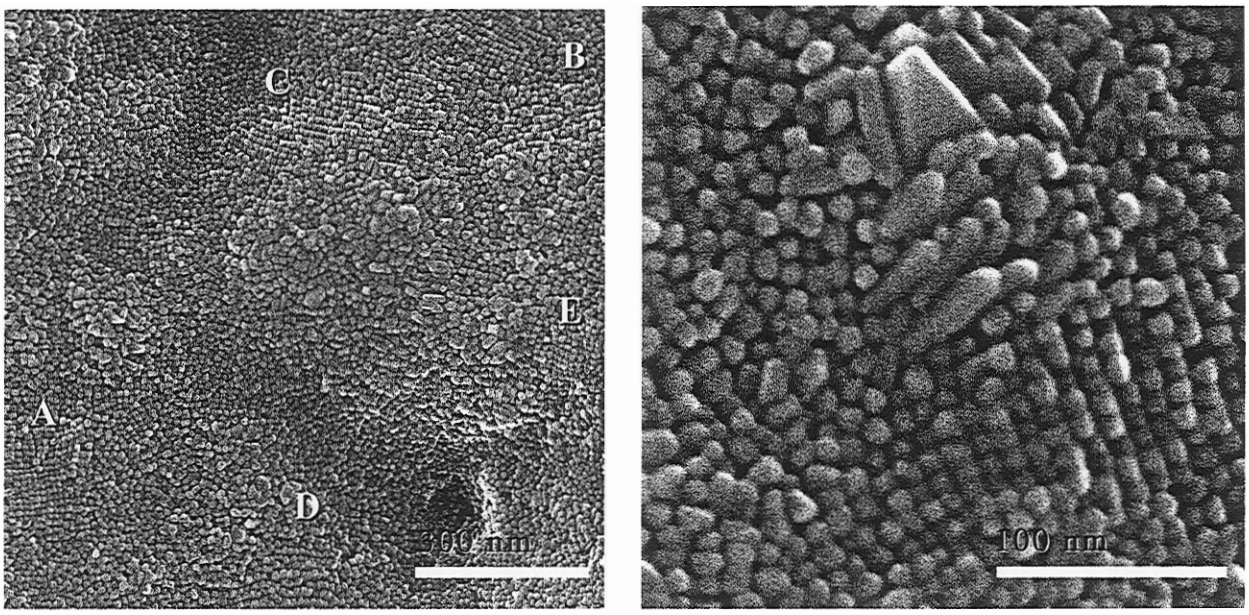

Figure 4. SEM micrographs of pseudo-square-bipyramidal TiO_2 particles with a maximum number of four neighbors in the equatorial plane. Two patterns (a) and (b) are taken at two different magnifications. More ordered regions of the pattern (a) are indicated.

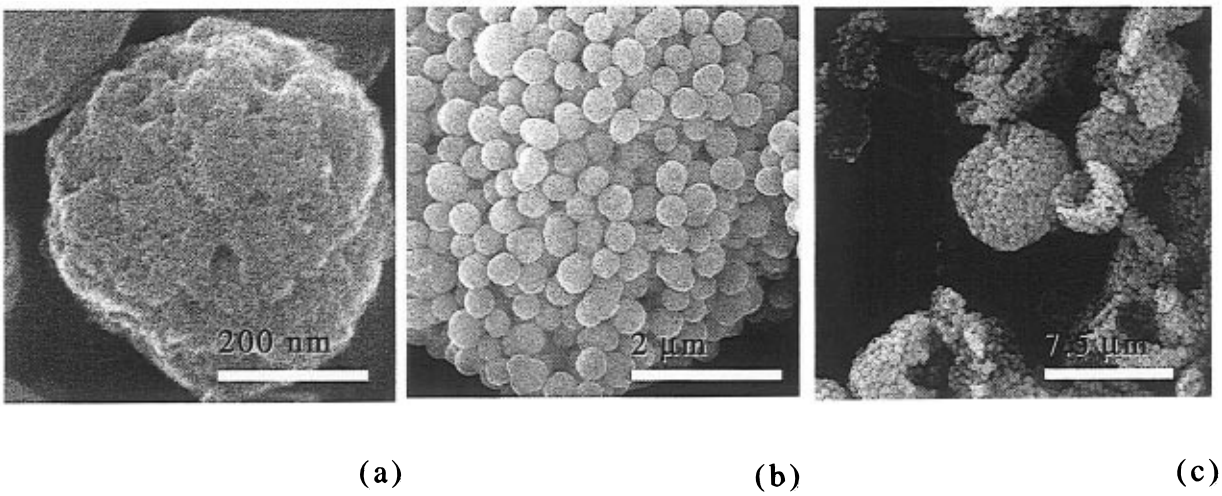

Figure 5. SEM micrographs illustrating three levels (a−c) of structural organization of the powder consisting of "large" nanocrystalline TiO_2 particles.

generating thin (∼150 nm) dense layers of (Cu) nanoclusters with a much broader cluster sizes distribution.[31]

The lattice-controlled topotactical interaction was found on the basis of a TEM study of the solid-state chemical conversion of perovskite $CaTiO_3$ to TiO_2 anatase and TiO_2 rutile.[32] The observed direct growth of TiO_2 in specific orientations is consistent with the proposed mechanism of this solid-state reaction, which involves direct structural inheritance of the parts of the framework of perovskite $CaTiO_3$.

Crystal Structure of Ru(etcbpy)$_2$(NCS)$_2$ (2). The molecular structure of the ester form of sensitizer Ru(etcbpy)$_2$(NCS)$_2$ (**2**) is shown in Figure 6. The *cis*-Ru(etcbpy)$_2$(NCS)$_2$ molecules have the crystallographic C_2 symmetry like in the crystal of [(2,2′-bpy)(NCS)]$_2$Ru (**4**, solvate with CH_3CN).[18] In the second known crystal structure of Ru(bpy)$_2$(NCS)$_2$ (**5**, solvate with $(CH_3)_2SO$)) the molecules occupy general positions.[18] The Ru atoms in all three *cis*-thiocyanate complexes **2**, **4**, **5** have a very similar somewhat distorted octahedral coordination (Table 5). Small differences in the Ru−N separations, more essential in the bond angles N−Ru−N and dihedral angles between the bpy ligands characterize the geometrical flexibility of the coordination surroundings of Ru atoms in the complexes Ru(bpy)$_2$(NCS)$_2$.

In the crystal structure of **2** the molecules Ru(etcbpy)$_2$(NCS)$_2$ form layers parallel to the *bc* plane of the crystal with interlayer separations of $b = 10.22$ Å, the solvate molecules CH_3CN are located between the layers (Figure 7). The shortest Ru···Ru separations are within one metal complexes layer of the crystal **2**·CH_3CN: 8.056 Å between the Ru atoms of the molecules related by the

(31) Haglund, R. F., Jr.; Nagruder, R. H., III; Yang, L.; Wittig, J. E.; Zuhr, R. A. *Physics and Chemistry of Finite Systems: From Clusters to Crystals*; Vol. II, 1992, Kluwer Academic Publishers: Dordrecht, p 1239.

(32) Banfield, J. F.; Veblen, D. R. *Am. Mineral.* **1992**, *77*, 545.

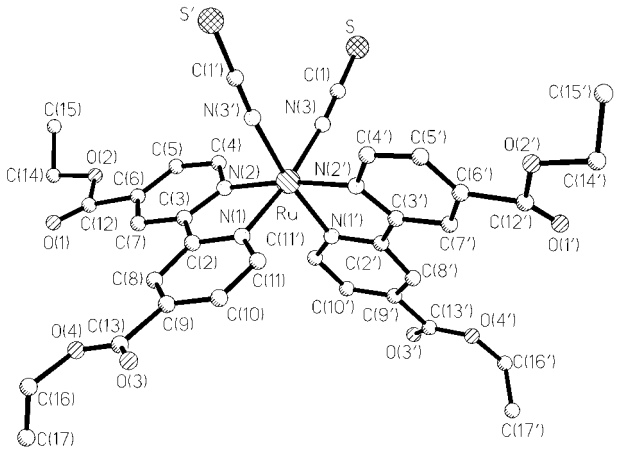

Figure 6. Molecular structure of the precursor **2**, projection parallel to the *a* axis of the crystal **2**.

Table 5. Comparison of Structures of *cis*-[(bpy)L]$_2$Ru Complexes in the Crystals of 2, 4, and 5

	2[a]	**4**[b]	**5**[b]
Ru−N(NCS)	2.07(2)	2.055(5)	2.052(6)
			2.059(5)
Ru−N(bpy)$_{cis}$	2.04(2)	2.041(4)	2.025(5)
			2.039(5)
Ru−N(bpy)$_{trans}$	2.01(1)	2.051(4)	2.055(5)
			2.059(6)
N(NCS)−Ru−N(NCS)′	86(1)	88.7(3)	91.3(2)
N(bpy)$_{trans}$−Ru−N(bpy)$_{cis}$[c]	78.3(7)	78.72)	79.1(2)
			79.3(3)
N(bpy)$_{trans}$−Ru−N(bpy)$_{trans}$[c]	95(1)	90.7(2)	91.9(2)
N(bpy)$_{cis}$−Ru−N(bpy)$_{cis}$[c]	172(1)	173.02)	175.0(2)
bpy/bpy[d]	81.1	86.49(7)	84.9(1)
py/py[e]	2.8	6(2)	4(1), 5(1)

[a] This work. [b] Reference 18. [c] N(bpy)$_{cis}$ and N(bpy)$_{trans}$ refer to the N(bpy) to the bpy ligand atoms cis and trans to the NCS ligand. [d] Dihedral angle between the mean planes of bipyridine ligands. [e] Dihedral angle between the pyridine planes of bipyridine ligands.

inversion center at (0,$^1/_2$,0) and (0,$^1/_2$,$^1/_2$), 10.229 Å between the molecules related by the $+b$ and $-b$ translations and 12.553 Å between the molecules related by the symmetry center at (0,0,0) and (0,0,$^1/_2$). Taking into account these shortest Ru···Ru separations, every Ru atom in the crystal Ru(etcbpy)$_2$(NCS)$_2$·CH_3CN is surrounded by eight Ru atoms of the same layer. The layered structure and the cocrystallization with solvate molecules are characteristic in the crystals of bipyridine metal complexes. Examples are crystal of tris(4,4′-dimethoxy-2,2′-bipyridine)iron(II) bis(hexafluorophosphate) (**6**, the cations are forming layers and the PF_6^- anions and solvate molecules of *N*-methyl-2-pyrrolidone are located between the layers),[33] crystal of the related complex bis(2,6-bis(1′-methylbenzimidazol-2′-yl)pyridine)cobalt(II) bis(hexafluorophosphate), solvate with 4-methyl-1,3-dioxolan-2-on (**7**, the anions PF_6^- and solvate molecules are located between the layers of metal complexes)[34] and the crystal of [Fe(bzimpy)$_2$](CF_3SO_3)·2EtOH (**8**).[35] Crystals of **6** are very stable; crystals **7** and **8** are losing solvent and become polycrystalline in the air. The removal of solvent molecules from the interlayered separations of crystalline bipyridine metal complexes may proceed (a) in a stepwise fashion and (b) topotactically with the conservation of layered motives of metal complexes, like it was shown by the TGA and powder diffraction study of solid-state (partial) desolvation of the crystals **7**.[34] Both observations (a) and (b) may be very important also for the understanding of properties of bipyridine metal complexes as sensitizers of porous nanocrystalline films, taking into account that, e.g., the crystal **7**, cocrystallized with the electrolyte 4-methyl-1,3-dioxolan-2-on as solvent, may be considered as a precursor of corresponding electrolyte system with the $(CoL_2)^{2+}/(CoL_2)^{3+}$ redox pair (L = bis-(2,6-bis(1′-methylbenzimidazol-2′-yl)pyridine).

In the crystal **2** close intermolecular contacts between the terminal S atoms of thiocyanato ligands and atoms of peripheral acetoxy substituents at bpy ligands of the same layer draw attention (the contact S···C(13) is even shorter as the sum of the van der Waals radii, see Table 6). This indicates a polar character of thiocyanato ligands at the Ru atoms and consequently may assume a participation of thiocyanato ligands to the interaction of complexes [Ru(dcbpy)$_2$(NCS)$_2$] with polar inorganic surfaces. Another kind of specific intermolecular interaction of bpy metal complex molecules was observed in the crystals **4**, where the C···C contacts of 3.352(9) and 3.524(8) Å between the bipyridine groups were suggested to be considered as plane−plane stacking interactions,[18] and **6**, where the indications of intermolecular $\pi-\pi$ stacking interactions of the types bipyridine···bipyridine were found out.[33] On the other hand, in crystals of other bpy and related metal complexes, e.g., in the crystal **7**,[34] the intermolecular interactions of the metal complex molecules are weaker and the shortened intermolecular contacts of metal complex molecules are absent.

Every molecule in the crystal **2** forms two contacts C(11)···N(4) with two solvent molecules CH_3CN, related by a 2-fold axis, at the separations of 3.83(3) Å, which are close to the sum of the van der Waals radii of C and N atoms and indicate a rather strong fixation of solvent CH_3CN molecules in the lattice. In the crystal **6**, the intermolecular $\pi-\pi$ interactions of metal complex molecule with the solvent molecules bipyridine···*N*-methyl-2-pyrrolidone were also found. In the crystal **7** the solvent molecules 4-methyl-1,3-dioxolan-2-one form close intermolecular contacts only with the PF_6^- anions within the interlayer separations and not with the metal complex cations.

Geometry of Anchoring of Sensitiser 3 to the Anatase Surfaces. Within one layer of the crystal **2**, every molecule (Ru(etcbpy)$_2$(NCS)$_2$) is surrounded by four other mutually centrosymmetrically related head-to-tail oriented molecules **3**. Hence, the layered arrangement of complexes Ru(etcbpy)$_2$(NCS)$_2$ in the crystal **2** cannot be used as a simple model for a positioning of sensitizer molecules on the polar TiO_2 surface. The second limitation for the use of the crystal structure **2** for the modeling is a decrease of dimensions of dianion **2** due to the removal of terminal ethyl groups. Nevertheless, the rigid geometry of the ligand surrounding in the complex **2** and the observed coplanarity of the terminal carboxy groups with corresponding pyridine rings (torsion angles C(5)C(6)C(12)O(2) and C(8)C(9)C(13)O(4) are 5.5 and 2.9°, respectively) allow an estimation of

(33) Shklover, V.; Nesper, R.; Zakeeruddin, S. M.; Fraser, D. M.; Grätzel, M. *Inorg. Chim. Acta* **1996**, *247*, 237.
(34) Shklover, V.; Eremenko, I. L.; Berke, H.; Nesper, R.; Zakeeruddin, S. M.; Nazeeruddin, Md. K.; Grätzel, M. *Inorg. Chim. Acta* **1994**, *219*, 11.
(35) Rüttiman, S.; Moreau, C. M.; Williams, A. F.; Bernardinelli, G.; Addison, A. W. *Polyhedron* **1992**, *11*, 635.
(36) Bondi, A. *J. Phys. Chem.* **1964**, *68*, 441.

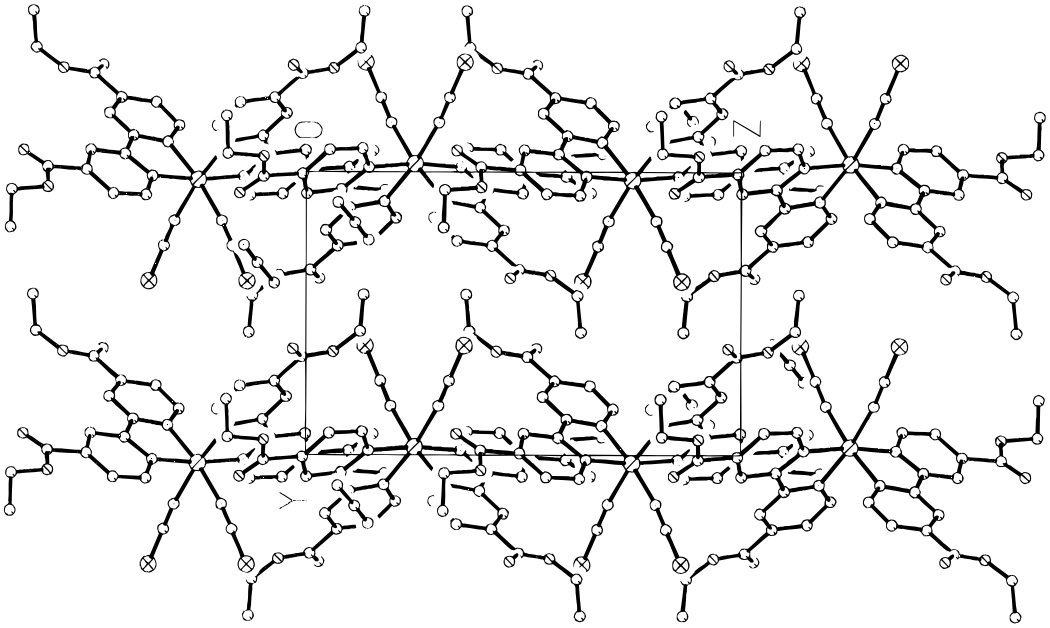

Figure 7. Layered structure of the crystal **2**, projection along the *a* axis.

Table 6. Shortest Intermolecular Separations *d* (Å) of Non-Hydrogen Atoms in the Crystal 2

	d		*d*
S···O(3)($-x,y-1,{}^1/_2-z$)	3.47(2)	S···O(4)($-x,y-1,{}^1/_2-z$)	3.672(2)
S···C(9)($-x,y-1,{}^1/_2-z$)	3.73(1)	S···C(13)($-x,y-1,{}^1/_2-z$)	3.44(3)[a]
O(1)···C(1)($x,1-y,{}^1/_2+z$)	3.42(3)	O(3)···C(5)($-x,1-y,1-z$)	3.34(4)
O(4)···C(1)($x,1-y,{}^1/_2+z$)	3.28(3)[a]	O(4)···C(4)($-x,1-y,1-z$)	3.38(4)
N(2)···C(11)($-x,y,{}^1/_2-z$)	3.18(3)[a]	N(3)···C(2)($-x,y,{}^1/_2-z$)	3.44(4)
C(5)···C(13)($-x,1-y,1-z$)	3.29(4)[a]	C(6)···C(9)($-x,1-y,1-z$)	3.43(4)[a]
C(10)···C(12)($-x,1-y,1-z$)	3.46(4)[a]	C(11)···N(4)($-x,1-y,1-z$)	3.38(3)[b]

[a] Shorter than the corresponding sum of van der Waals radii. The sums of the van der Waals radii are 3.32 Å for S + O, 3.50 Å for S + C, 3.32 Å for O + C, 3.35 Å for N + C, 3.60 Å for C + C.[36] [b] Contact of the molecule [(dcobpy)(NCS)]$_2$Ru with the solvent molecule CH_3CN.

Table 7. Intramolecular Distances *D*(O···O) (Å) in the Molecule 2

	D		*D*
O(1)···O(1)	13.76	O(2)···O(3)	9.94
O(1)···O(2)	2.25	O(2)···O(3′)	9.92
O(1)···O(2′)	13.73	O(2)···O(4)	8.18
O(1)···O(3)	8.29	O(2)···O(4′)	11.28
O(1)···O(3′)	10.39	O(3)···O(3′)	11.20
O(1)···O(4)	6.33	O(3)···O(4)	2.25
O(1)···O(4′)	11.59	O(3)···O(4′)	10.93
O(2)···O(2′)	13.82	O(4)···O(4′)	11.12

both parameters, characterizing a geometry of anchoring of **3**: (a) the intramolecular O···O separations (Table 7) and (b) the van der Waals surface area of the sensitizer **3** on the semiconductor surface for different types of anchoring (Figure 8, Table 8).

The anchoring of sensitizer **3** to the TiO_2 surface via one or two carboxy groups is more probable than via one or four groups. The anchorings of **3** via the carboxy groups O(1)C(12)O(2) (a1) and O(3)C(13)O(4) (a2) are nonequivalent: the molecular surface areas are significantly different (121 and 86 Å^2, Figure 8) at the same O···O bite sizes of 2.25 Å (Tables 7 and 8). There are five possibilities for the bonding of the sensitizer **3** to the TiO_2 particle via two carboxy groups, four of which (a3−a6) are symmetrically independent and may be characterized by different surface areas of 97−130 Å^2. Simultaneous bonding via the groups O(1)O(2) and O(1′)O(2′) is probably negligible. Using the intramolecular O···O separations from the Table 7, the bites a3, a4, and a5 may be determined as 11.1, 8.2, and 10.8 Å.

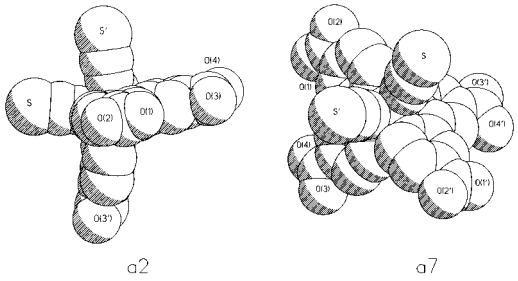

Figure 8. Space-filling models of dianione **3**, anchored to TiO_2 surface through one carboxy group at C(12) ipso atom (anchoring a2) and through three carboxy groups at C(12), C(13), and C(13′) ipso atoms (anchoring a7). Anchoring a2 corresponds to the smallest (86 Å^2), anchoring a7 to one of the largest (130 Å^2) surface areas of dianinone **3** on TiO_2 surface; see Table 8.

The surface area of **3** for the only possible anchoring via three carboxy groups a7 is the same as for anchoring type a8 via four carboxy groups. The anchoring via four carboxy groups is hindered for the flat TiO_2 surface.

The terminal CO_2H groups in **3** may bring also to the lateral assembling interactions of sensitizer molecules **3** (see, e.g., discussion[37] of self-assembling of alkanethiolates on Au(111)). Another limitation of discussed model of the anchoring of sensitizer **3** is coming from the experimental HRTEM study,[24] which shows that an essential amount of metal particles in the Rh/TiO_2

(37) Allara, D. L. In *Atomic and Nanometer Scale Modification of Materials: Fundamentals and Applications*; Avouris, P., Ed.; Kluwer Academic Publishers: Dordrecht, 1993; p 275.

Table 8. Surface Area of Dianione 3 for Different Types of Anchoring (See Also Figure 8)

anchoring[a]	N[b]	anchoring carboxy groups[c]	surface (Å^2)[d]
a1	1	C(13)	121
a2	1	C(12)	86
a3	2	C(12), C(13)	97
a4	2	C(12), C(12′)	130[e]
a5	2	C(13), C(13′)	130[e]
a6	2	C(12), C(13′)	108
a7	3	C(12), C(13), C(13′)	127[f]
a8	4	C(12), C(13), C(12′), C(13′)	130[e]

[a] Only symmetrically independent anchorings are given, assuming C_2 symmetry of the dicatione **2**. [b] Number of anchoring carboxy groups. [c] Only ipso atoms of carboxy groups are given. [d] The surface area analysis was performed on a PowerMacintosh 7100 computer using the public domain NIH Image program (developed at the U.S. National Institutes of Health and available from the Internet by anonymous FTP from zippy.nimh.nih.gov or on floppy disk from the National Information Service, Springfeld, Virginia, part no. PB95-500195GEI). [e] Dianione **3** oriented for the anchorings a4, a5, and a8 has the same surface area on the semiconductor surface. [f] The second symmetrically independent anchoring via three carboxy groups C(12), C(13), and C(12′) is impossible due to steric reasons.

catalysts were located on the edges of the TiO_2 crystallites. Such positioning of **3** makes possible also the a4, a5, and a8 types of anchoring. We intend to perform the simulation of location and bonding of the sensitizer **3** on the TiO_2 anatase surface in due course.

Conclusion

On the basis of our HRTEM study, the termination of the anatase nanocrystallites with the planes (101), (010), and (to less extent) (001) was found to be very likely for the TiO_2 colloid films autoclaved at 240 °C. The HRTEM and SEM studies show the bipyramidal habitus of TiO_2 nanocrystallites treated at 240 °C as a dominant one. New examples are given for the formation of dense packing of nanocrystals: the pseudospherical ZnO particles are forming hexagonal packing with the maximum number of neighbors 12 (six in the equatorial plane), the pseudo-square-bipyramidal TiO_2 nanoparticles are packed with the maximum number of four neighbors in the equatorial plane, which can prevent the faces (001) of corresponding sintered nanocrystalline film from the interaction with the sensitizer. Depending on the method of preparation, the "large" TiO_2 nanocrystallites may form associates with an unusual hollow structure. The X-ray single-crystal structure investigation of the precursor of sensitizer *cis*-$Ru(etcbpy)_2(NCS)_2$, performed at 210 K, shows that the molecules have the crystallographic C_2 symmetry and are packed into the layered structure with the layers parallel to the bc plane of the crystal, interlayered separations of 10.23 Å, and with solvent CH_3CN located between the layers. Somewhat shorter intermolecular contacts of S atoms of thiocyanato ligands with peripheral aceto substituents in the crystal of precursor may indicate a possibility of participation of thiocyanato groups in the electrostatic interaction during the formation of sensitizing coating. The surface area of the sensitizer *cis*-$Ru(dcbpy)_2(NCS)_2$ varies from 86 to 130 Å^2 for different types of anchoring to the semiconductor's surface.

Acknowledgment. We are indebted to the Swiss Energy Office, Project EF-REN (91)054, and the Swiss Commission for the Encouragement of Scientific Research, Project 2442, for financial support.

CM950502P